

Disentangling the high and low cutoff scales via the trilinear Higgs couplings in the type-I two-Higgs-doublet model

Sin Kyu Kang,^{1,*} Jinheung Kim,^{2,†} Soojin Lee,^{2,‡} and Jeonghyeon Song^{2,§}

¹*School of Liberal Arts , Seoul-Tech, Seoul 139-743, Korea*

²*Department of Physics, Konkuk University, Seoul 05029, Republic of Korea*

Abstract

The type-I two-Higgs-doublet model in the inverted Higgs scenario can retain the theoretical stability all the way up to the Planck scale. The Planck-cutoff scale, $\Lambda_{\text{cut}}^{\text{Planck}}$, directly impacts the mass spectra such that all the extra Higgs boson masses should be light below about 160 GeV. However, the observation of the light masses of new Higgs bosons does not indicate the high cutoff scale because a low cutoff scale can also accommodate the light masses. Over the viable parameter points that satisfy the theoretical requirements and the experimental constraints, we show that the trilinear Higgs couplings for low Λ_{cut} are entirely different from those for the Planck-cutoff scale. The most sensitive coupling to the cutoff scale is from the h - h - h vertex, where h is the lighter CP -even Higgs boson at a mass below 125 GeV. Among the multi-Higgs productions mediated by Higgs bosons, the gluon fusion processes of $gg \rightarrow hh$ and $gg \rightarrow AA$ are insensitive to the cutoff scale, yielding a small variation of $\mathcal{O}(1)$ fb according to Λ_{cut} . The smoking-gun signature is from the triple Higgs production of $q\bar{q}' \rightarrow W^* \rightarrow H^\pm hh$, which solely depends on the h - h - h vertex. The cross section for $\Lambda_{\text{cut}} = 1 \text{ TeV}$ is about 10^3 times larger than that for the Planck-cutoff scale. Since the decay modes of $H^\pm \rightarrow W^*h/W^*A$ and $h/A \rightarrow bb$ are dominant, the process yields the $6b + \ell\nu$ final state, which enjoys an almost background-free environment. Consequently, the precision measurement of $pp \rightarrow H^\pm hh$ can probe the cutoff scale of the model.

arXiv:2210.00020v1 [hep-ph] 30 Sep 2022

*Electronic address: skkang@snut.ac.kr

†Electronic address: jinheung.kim1216@gmail.com

‡Electronic address: soojinlee957@gmail.com

§Electronic address: jhsong@konkuk.ac.kr

Contents

I. Introduction	2
II. Review of type-I of 2HDM in the inverted scenario	4
III. Scanning and RGE analysis	6
IV. Trilinear Higgs couplings and the LHC phenomenology	10
V. Conclusion	16
Acknowledgments	17
A. RGEs in the type-I 2HDM	17
References	19

I. INTRODUCTION

Up to today, all of the measurements of the production cross sections of the standard model (SM) particles at high energy colliders are in good agreement with the SM predictions [1], including the observed Higgs boson with a mass of 125 GeV [2–16]. Nevertheless, our minds are rarely in satisfaction with the SM because of the unsolved questions of the naturalness problem, baryogenesis, non-zero neutrino masses, fermion mass hierarchy, the origin of CP violation in the quark sector, and the identity of dark matter. So, we continue our journey in the quest of the ultimate theory. To answer the fundamental questions, we need one specific model, although the indirect method resorting to the SMEFT [17–20] systematically characterizes the new physics (NP) structure via the experimental deviations from the SM predictions.

The next question we address is whether the ultimate theory shall reveal its whole structure at one energy scale. When looking back on the SM, the only reliable guideline at this moment, the answer is much more likely to be *no*. We had witnessed the emergence of SM particles in stages. The same phenomena could happen in the ultimate theory. In other words, the final theory may consist of multilevel sub-models, and we are destined to discover new particles one by one as we increase the energy scale. The first-stage NP model describes our universe up to a certain energy scale Λ_{cut} and then hands over its role to the second-stage NP model, and so on. The Λ_{cut} of the first-stage NP model could be as high as the GUT scale or as low as 10 TeV. Then can an observable distinguish the high and low Λ_{cut} ? This is the driving question in our paper.

For the first-stage NP model, we consider the two-Higgs-doublet model (2HDM) since many fundamental questions are closely related to the Higgs sector. The 2HDM provides the answers to some questions. For example, the baryogenesis can be explained by the first-order electroweak

phase transition in the 2HDM [21–25]. However, the model cannot address all the fundamental questions, which makes it a suitable candidate for the first-stage NP model.

Then the next question is how to calculate the energy scale at which the second-stage NP model appears. A good way is to calculate the cutoff scale of the 2HDM. Even though a parameter point retains the theoretical stability (unitarity, perturbativity, and vacuum stability) at the electroweak scale, a stability condition can be broken at a higher energy scale Λ_{cut} because the parameters evolve under renormalization group equations (RGE) [26–32]. The broken validity of the first-stage model implies the advent of the second-stage model. Thus we call Λ_{cut} the cutoff scale of the model. In this paper, we focus on the type-I in the inverted scenario where the heavier CP -even scalar H is the observed one [33–35]. In the inverted scenario, type-I can accommodate the cutoff scale all the way up to the Planck scale [36].

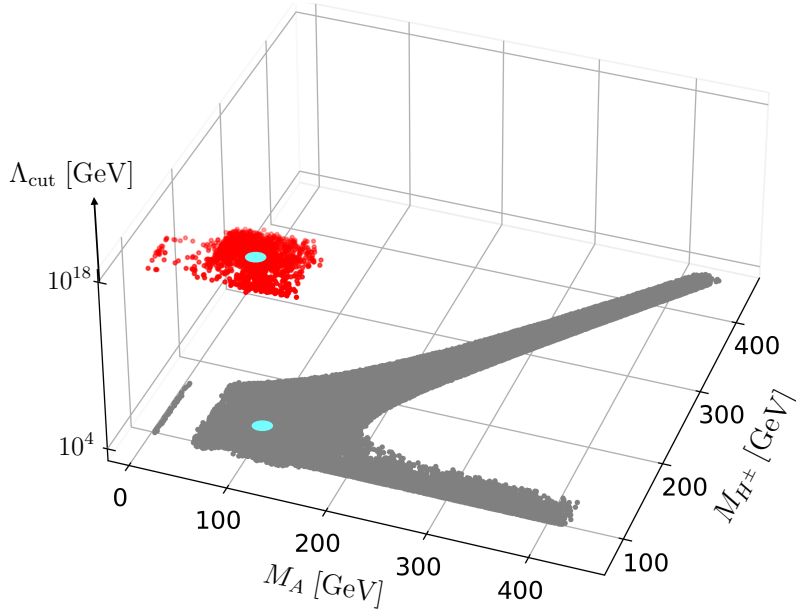


FIG. 1: Allowed (M_A, M_{H^\pm}) with the cutoff scales of $\Lambda_{\text{cut}} = 10$ TeV (gray points) and $\Lambda_{\text{cut}} \geq 10^{18}$ GeV (red points) in the inverted type-I 2HDM, over the viable parameter points that satisfy the theoretical requirements and the experimental constraints. Two points in cyan yield the same M_A and M_{H^\pm} .

In the literature, the high-energy scale behavior of the 2HDM has been extensively studied, mostly on the possibility of high Λ_{cut} and the high scale impact on the extra Higgs boson masses [30, 36–44]. However, observing the scalar mass spectrum that the high Λ_{cut} predicts does not indicate that Λ_{cut} is high. As illustrated in Fig. 1, the allowed points of (M_A, M_{H^\pm}) for $\Lambda_{\text{cut}} = 10$ TeV (gray points) are overlapped with those for $\Lambda_{\text{cut}} = 10^{18}$ GeV (red points). Two points in cyan have the same M_A and M_{H^\pm} , which both $\Lambda_{\text{cut}} = 10$ TeV and $\Lambda_{\text{cut}} = 10^{18}$ GeV accommodate. We need an alternative observable to disentangle the high and low cutoff scales. The measurement of $\tan \beta$, the ratio of two vacuum expectation values of two Higgs doublet fields, is tricky in type-I when $\tan \beta \gg 1$, if we consider only the dominant observables such as

$gg \rightarrow A/h$ and $t \rightarrow H^\pm b$. In type-I, all the Yukawa couplings are inversely proportional to $\tan \beta$ in the Higgs alignment limit. So, the gluon fusion production of a single extra Higgs boson via top quark loop is suppressed by large $\tan \beta$ and the branching ratios of all the fermionic decay modes are insensitive to $\tan \beta$.

We will show that the trilinear Higgs couplings are different according to Λ_{cut} . In particular, the value of the h - h - h vertex, $\hat{\lambda}_{hhh}$, is susceptible to the cutoff scale. To exclusively probe $\hat{\lambda}_{hhh}$ at the LHC, we will study the di-Higgs processes of $gg \rightarrow hh$ and $gg \rightarrow AA$, and the tri-Higgs processes of $pp \rightarrow H^\pm hh$. The gluon fusion production cross section of $gg \rightarrow hh/AA$ is to be shown insensitive to Λ_{cut} because of the pollution from the H - h - h vertex. We will present that the tri-Higgs process $pp \rightarrow H^\pm hh$ is the best to measure the cutoff scale because the signal rate is highly sensitive to Λ_{cut} , like $\sigma_{\Lambda_{\text{cut}}=1 \text{ TeV}}/\sigma_{\Lambda_{\text{cut}}=10^{18} \text{ GeV}} \sim 10^3$. Considering the dominant decays modes of H^\pm and h , we will suggest for the first time the $6b + \ell\nu$ final state as an efficient discriminator between the high and low cutoff scales. These are our new contributions.

The paper is organized in the following way. In Sec. II, we briefly review the type-I of the 2HDM in the inverted scenario. Section III describes the methods of the parameter scanning and the calculation of Λ_{cut} . The characteristics of the viable parameter points with high Λ_{cut} are also presented. In Sec. IV, we calculate the correlation between the trilinear Higgs couplings and the cutoff scale. Based on the study of the branching ratios of the extra Higgs bosons, we will suggest efficient observables to distinguish the high and low cutoff scales. Finally we conclude in Sec. V.

II. REVIEW OF TYPE-I OF 2HDM IN THE INVERTED SCENARIO

The 2HDM introduces two $SU(2)_L$ complex scalar doublet fields with hypercharge $Y = 1$, Φ_1 and Φ_2 [45]:

$$\Phi_i = \begin{pmatrix} w_i^+ \\ \frac{v_i + \rho_i + i\eta_i}{\sqrt{2}} \end{pmatrix}, \quad (i = 1, 2) \quad (1)$$

where v_1 and v_2 are the nonzero vacuum expectation values of Φ_1 and Φ_2 , respectively. The ratio of v_2/v_1 defines the mixing angle β via $\tan \beta = v_2/v_1$. For notational simplicity, we use $s_x = \sin x$, $c_x = \cos x$, and $t_x = \tan x$ in what follows. The combination of v_1 and v_2 , $v = \sqrt{v_1^2 + v_2^2} = 246 \text{ GeV}$, spontaneously breaks the electroweak symmetry. To prevent flavor-changing neutral currents at tree level, we impose a discrete Z_2 symmetry under which $\Phi_1 \rightarrow \Phi_1$ and $\Phi_2 \rightarrow -\Phi_2$ [46, 47]. We allow softly broken Z_2 symmetry since it does not affect the RGE of the dimensionless quartic couplings [48]: the hard Z_2 breaking in the Yukawa sector causes too fast growth of the scalar quartic couplings in the RG running [40].

With the CP invariance, the scalar potential is written as

$$\begin{aligned}
V_\Phi = & m_{11}^2 \Phi_1^\dagger \Phi_1 + m_{22}^2 \Phi_2^\dagger \Phi_2 - m_{12}^2 (\Phi_1^\dagger \Phi_2 + \text{H.c.}) \\
& + \frac{1}{2} \lambda_1 (\Phi_1^\dagger \Phi_1)^2 + \frac{1}{2} \lambda_2 (\Phi_2^\dagger \Phi_2)^2 + \lambda_3 (\Phi_1^\dagger \Phi_1) (\Phi_2^\dagger \Phi_2) + \lambda_4 (\Phi_1^\dagger \Phi_2) (\Phi_2^\dagger \Phi_1) \\
& + \frac{1}{2} \lambda_5 \left[(\Phi_1^\dagger \Phi_2)^2 + \text{H.c.} \right],
\end{aligned} \tag{2}$$

where the m_{12}^2 term softly breaks the Z_2 symmetry. The scalar potential V_Φ yields five physical Higgs bosons, the lighter CP -even scalar h , the heavier CP -even scalar H , the CP -odd pseudoscalar A , and a pair of charged Higgs bosons H^\pm . Relations of mass eigenstates with weak eigenstates in terms of two mixing angles of α and β are referred to Ref. [49]. The SM Higgs boson is a linear combination of h and H , given by

$$h_{\text{SM}} = s_{\beta-\alpha} h + c_{\beta-\alpha} H. \tag{3}$$

The observed Higgs boson at a mass of 125 GeV at the LHC [2–16] has so far agreed with the predictions for the SM Higgs boson. The SM-like Higgs boson strongly motivates the Higgs alignment limit in the 2HDM. Two scenarios exist for the limit, the normal scenario where $h_{\text{SM}} = h$ (i.e., $s_{\beta-\alpha} = 1$) and the inverted scenario where $h_{\text{SM}} = H$ (i.e., $c_{\beta-\alpha} = 1$). In this paper, we concentrate on the inverted scenario in the Higgs alignment limit:

$$M_H = 125 \text{ GeV}, \quad c_{\beta-\alpha} = 1. \tag{4}$$

Then we have the following five parameters:

$$\{m_h, \quad M_A, \quad M_{H^\pm}, \quad t_\beta, \quad m_{12}^2\}, \tag{5}$$

which defines one parameter point. Then, the quartic coupling constants in V_Φ are written as [50]

$$\begin{aligned}
\lambda_1 &= \frac{1}{v^2} [m_{125}^2 + t_\beta^2 (m_h^2 - M^2)], \\
\lambda_2 &= \frac{1}{v^2} \left[m_{125}^2 + \frac{1}{t_\beta^2} (m_h^2 - M^2) \right], \\
\lambda_3 &= \frac{1}{v^2} [m_{125}^2 - m_h^2 - M^2 + 2M_{H^\pm}^2], \\
\lambda_4 &= \frac{1}{v^2} [M^2 + M_A^2 - 2M_{H^\pm}^2], \\
\lambda_5 &= \frac{1}{v^2} [M^2 - M_A^2],
\end{aligned} \tag{6}$$

where $m_{125} = 125 \text{ GeV}$ and $M^2 = m_{12}^2 / (s_\beta c_\beta)$.

The Yukawa couplings to the SM fermions are parametrized as

$$\begin{aligned}
\mathcal{L}^{\text{Yuk}} = & - \sum_f \left(\frac{m_f}{v} \xi_f^h \bar{f} f h + \frac{m_f}{v} \kappa_f^H \bar{f} f H - i \frac{m_f}{v} \xi_f^A \bar{f} \gamma_5 f A \right) \\
& - \left\{ \frac{\sqrt{2}}{v} \bar{t} (m_t \xi_t^A P_- + m_b \xi_b^A P_+) b H^+ + \frac{\sqrt{2} m_\tau}{v} \xi_\tau^A \bar{\nu}_\tau P_+ \tau H^+ + \text{H.c.} \right\},
\end{aligned} \tag{7}$$

which are different according to the 2HDM type. In this work, we focus on type-I. To facilitate the discussion below, we will call the type-I with the conditions of Eq. (4) the inverted type-I. Then the Higgs coupling modifiers are

$$\xi_f^H = 1, \quad \xi_{t,b,\tau}^h = \frac{1}{t_\beta}, \quad \xi_t^A = -\xi_{b,\tau}^A = \frac{1}{t_\beta}. \quad (8)$$

The trilinear Higgs couplings as dimensionless parameters are defined by

$$\begin{aligned} \mathcal{L}_{\text{tri}} = \sum_{\varphi_0=h,H} v \left\{ \frac{1}{3!} \hat{\lambda}_{\varphi_0\varphi_0\varphi_0} \varphi_0^3 + \frac{1}{2} \hat{\lambda}_{\varphi_0AA} \varphi_0 A^2 + \lambda_{\varphi_0H^+H^-} \varphi_0 H^+ H^- \right\} \\ + \frac{1}{2} \hat{\lambda}_{Hhh} v H h^2 + \frac{1}{2} \hat{\lambda}_{hHH} v h H^2. \end{aligned} \quad (9)$$

In the inverted type-I, the couplings are

$$\begin{aligned} \hat{\lambda}_{HHH} &= -\frac{3m_{125}^2}{v^2}, \quad \hat{\lambda}_{hHH} = 0, \\ \hat{\lambda}_{hhh} &= 3\hat{\lambda}_{hAA} = 3\hat{\lambda}_{hH^+H^-} = -\frac{3(M^2 - m_h^2)(t_\beta^2 - 1)}{t_\beta v^2}, \\ \hat{\lambda}_{Hhh} &= -\frac{m_{125}^2 + 2m_h^2 - 2M^2}{v^2}, \\ \hat{\lambda}_{HAA} &= -\frac{m_{125}^2 + 2M_A^2 - 2M^2}{v^2}, \\ \hat{\lambda}_{HH^+H^-} &= -\frac{m_{125}^2 + 2M_{H^\pm}^2 - 2M^2}{v^2}. \end{aligned} \quad (10)$$

The trilinear coupling of the observed Higgs boson H is the same as in the SM, $\hat{\lambda}_{HHH} \simeq 0.77$, because we adopt the Higgs alignment limit. Another remarkable feature is that $\hat{\lambda}_{hhh}$, $\hat{\lambda}_{hAA}$, and $\hat{\lambda}_{hH^+H^-}$ are dependent on each other, with the common factor proportional to $t_\beta(M^2 - m_h^2)$ in the large t_β limit.

III. SCANNING AND RGE ANALYSIS

Before studying the high energy behavior of the model via RGE, the preparation of the still-allowed parameter points at the electroweak scale is an essential prerequisite. Therefore, we randomly scan five model parameters in the range of

$$\begin{aligned} t_\beta \in [1, 50], \quad M_A \in [10, 3000] \text{ GeV}, \quad m_{12}^2 \in [-3000^2, 3000^2] \text{ GeV}^2, \\ M_{H^\pm} \in [80, 3000] \text{ GeV}, \quad m_h \in [10, 120] \text{ GeV}, \end{aligned} \quad (11)$$

and cumulatively impose the following constraints:

- **Theoretical requirements**

We demand the Higgs potential to be bounded from below [51], tree-level unitarity of scalar-scalar scatterings [45, 52], perturbativity [34], and the stability of the CP -conserving vacuum with $v = 246$ GeV [53–55].

- **Peskin-Takeuchi oblique parameters** [56]

The oblique parameters of S , T , and U in the 2HDM calculations [57–59] should satisfy the current best-fit results at 95% C.L. [59]:

$$\begin{aligned} S &= -0.01 \pm 0.10, \\ T &= 0.03 \pm 0.12, \quad U = 0.02 \pm 0.11, \\ \rho_{ST} &= 0.92, \quad \rho_{SU} = -0.80, \quad \rho_{TU} = -0.93, \end{aligned} \tag{12}$$

where ρ_{ij} is the correlation matrix.

- **Flavor changing neutral currents**

We demand that the most recent observables from B physics be satisfied at 95% C.L. [60–62].

- **Higgs precision data**

We use the public code HIGGSIGNALS-v2.6.2 [63] to check the consistency with the Higgs precision data. Based on the χ^2 value for 111 Higgs observables [64–71] with five parameters, we require that the p -value be larger than 0.05.

- **Direct search bounds**

We demand that the model prediction to the cross sections of the direct search modes for new scalar bosons at the LEP, Tevatron, and LHC should be less than 95% C.L. upper bound on the observed cross sections. The open code HIGGSBOUNDS-v5.10.2 [72] is used.

Brief comments on the recent CDF measurement of the W -boson mass [73], $m_W^{\text{CDF}} = 80.4335 \pm 0.0094$ GeV, are in order here. If we accept m_W^{CDF} , the oblique parameters change into $S_{\text{CDF}} = 0.15 \pm 0.08$ and $T_{\text{CDF}} = 0.27 \pm 0.06$ with $U = 0$ [74]. Although m_W^{CDF} has important implications on the 2HDM [36, 43, 74–87], our main conclusion on the role of trilinear Higgs couplings in disentangling the high and low cutoff scales does not change. So, we focus on the oblique parameters without the CDF m_W measurement.

Over the parameter points that pass the above constraints, we evolve the following parameters via the RGE, by using the public code 2HDME [40, 88]:

$$g_{1,2,3}, \quad \lambda_{1,\dots,5}, \quad \xi_f^{h,H,A}, \quad m_{11}, \quad m_{12}, \quad m_{22}^2, \quad v_{1,2}. \tag{13}$$

We include the mixing effects of two scalar doublet fields (with equal quantum numbers) on v_1 and v_2 , which brings about the RG running of t_β . The top quark pole mass scale, $m_t^{\text{pole}} = 173.4$ GeV, is used to match the 2HDM to the SM parameters. The boundary conditions at m_t^{pole} are referred to Ref. [40]. The β functions of the gauge, Yukawa, and quartic couplings at one loop level are presented in Appendix A. Since the difference between the one-loop and two-loop RG running is not large, we take the one-loop RGE to efficiently cover all the parameter points.

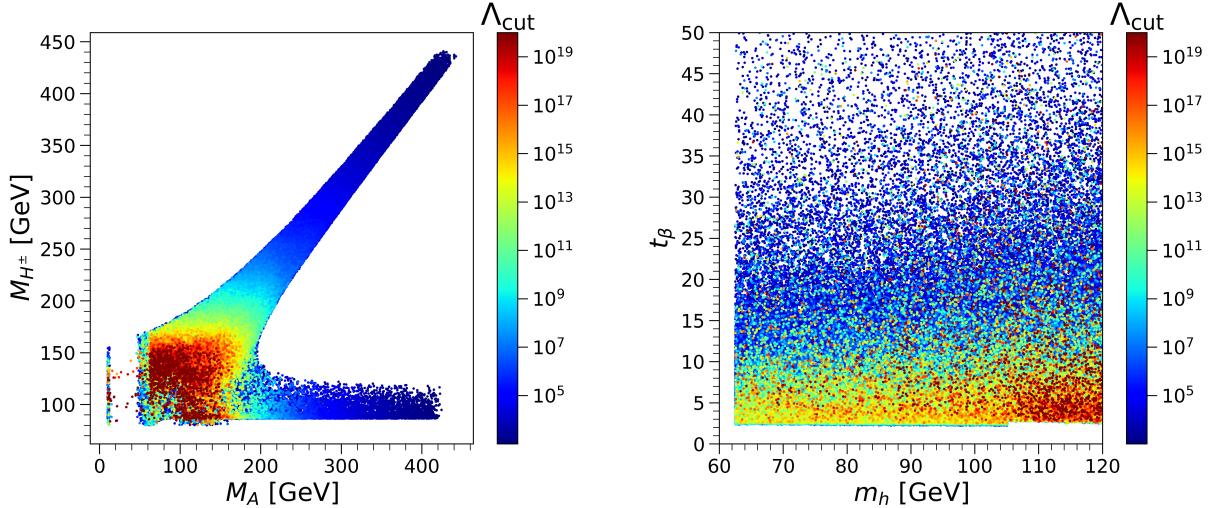


FIG. 2: M_{H^\pm} versus M_A in the left panel and t_β versus m_h in the right panel. The color code denotes the cutoff scale Λ_{cut} .

Now let us describe how we obtained the cutoff scale Λ_{cut} . For each viable parameter point, we perform the RGE evolution into the next high energy scale¹ and check three conditions, tree-level unitarity, perturbativity, and vacuum stability. If all three are satisfied, we increase the energy scale into the next step. If any condition is violated, we stop the running and record the energy scale as Λ_{cut} . We additionally require that the cutoff scale should be larger than 1 TeV. From now on, the “viable parameter points” denote the parameter points that satisfy the aforementioned constraints and $\Lambda_{\text{cut}} > 1$ TeV.

Strong correlations exist between the cutoff scale and the model parameters. In Fig. 2, we present the viable parameter points over the plane of (M_A, M_{H^\pm}) in the left panel and over (m_h, t_β) in the right panel. The color code denotes the cutoff scale Λ_{cut} . We sorted the viable parameter points according to Λ_{cut} , and stacked them in order of Λ_{cut} , the points with low Λ_{cut} underneath and those with high Λ_{cut} on top. The overlap is due to the projection of five-dimensional parameter space in Eq. (5) on a two-dimensional subspace.

Several remarkable features are shown in Fig. 2. First, the viable parameter points is quite limited even with the weak condition of $\Lambda_{\text{cut}} > 1$ TeV. The upper bounds on M_A and M_{H^\pm} exist as $M_A, M_{H^\pm} \lesssim 430$ GeV, to which the condition of $\Lambda_{\text{cut}} > 1$ TeV plays a critical role. For the intermediate mass range of $M_A, M_{H^\pm} \lesssim 200$ GeV, there is no particular correlation between M_A and M_{H^\pm} . However, a meaningful correlation exists in the range of $M_A \gtrsim 200$ GeV or $M_{H^\pm} \gtrsim 200$ GeV. If $M_{H^\pm} \gtrsim 200$ GeV, $M_{H^\pm} \simeq M_A$. If $M_{H^\pm} \lesssim 200$ GeV and $M_A \gtrsim 200$ GeV, $M_{H^\pm} \sim 100$ GeV. The lighter CP -even Higgs boson mass m_h (right panel of Fig. 2) should be heavier than half the observed Higgs boson mass due to the constraint from the exotic Higgs boson decay of $H \rightarrow hh$. For t_β , most values in the scanning are permitted. Although the

¹ To cover from the electroweak scale to the Planck scale, we take a uniform step in $\log(Q)$.

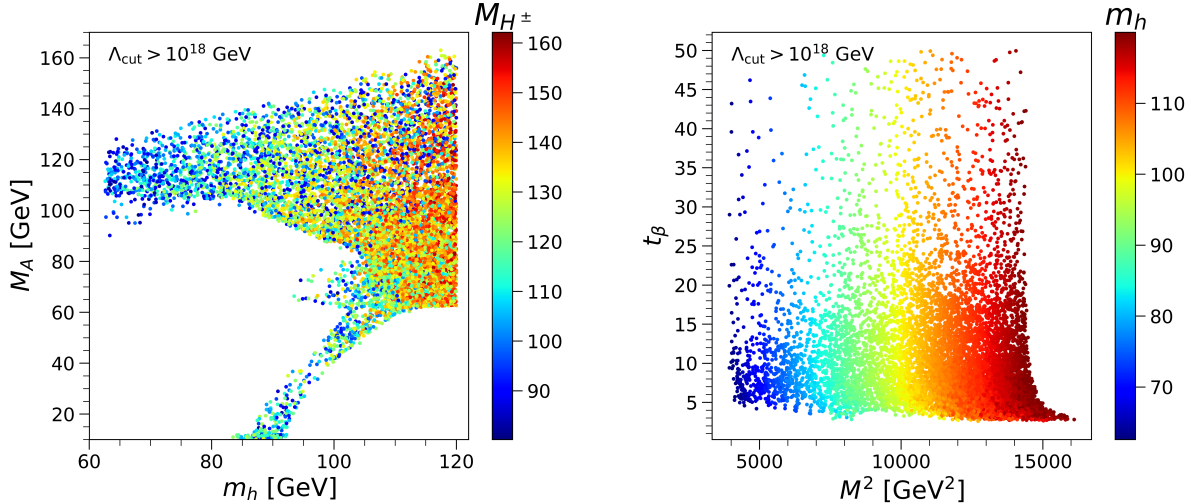


FIG. 3: For $\Lambda_{\text{cut}} > 10^{18}$ GeV, M_A versus m_h in the left panel and t_β versus M^2 in the right panel. The color code denotes M_{H^\pm} in the left panel and m_h in the right panel.

density of the allowed t_β in the scatter plot is higher for smaller t_β , we cannot conclude that small t_β is preferred: nature chooses just one parameter point.

The second remarkable feature of Fig. 2 is that some parameter points in the inverted type-I remain stable all the way up to the Planck scale. To reveal the characteristics of the parameter points with the high cutoff scale, we show in Fig. 3 M_A versus m_h (left panel) and t_β versus M^2 (right panel) after imposing $\Lambda_{\text{cut}} > 10^{18}$ GeV. The color code in the left (right) panel denotes M_{H^\pm} (m_h). It is clearly seen that the high cutoff scale requires *light* masses of the extra Higgs bosons like $M_A, M_{H^\pm} \lesssim 160$ GeV. We observe that the charged Higgs boson is lighter than the top quark for the Planck-scale cutoff. However, the lower bounds of $M_A \gtrsim 10$ GeV, $m_h \gtrsim 62.5$ GeV, and $M_{H^\pm} \gtrsim 80$ GeV do not change by imposing $\Lambda_{\text{cut}} > 10^{18}$ GeV. Similarly, the Planck-scale cutoff does not affect the values of t_β , as shown in the right panel of Fig. 3.

The values of M^2 are also limited even with $\Lambda_{\text{cut}} > 1$ TeV. Only the positive values of M^2 are permitted because negative M^2 excessively increase λ_1 through the terms proportional to t_β^2 , which endangers the global minimum condition of the vacuum [53–55]. Large λ_1 at the electroweak scale quickly evolves into an unacceptably large value that breaks the stability. We find that M^2 ranges from about $(40 \text{ GeV})^2$ to about $(125 \text{ GeV})^2$. If we further require $\Lambda_{\text{cut}} > 10^{18}$ GeV as shown in the right panel in Fig. 3, a unique correlation of $M^2 \simeq m_h^2$ appears. It is also ascribed to the t_β^2 terms in λ_1 . The condition of $M^2 \simeq m_h^2$ suppresses the t_β^2 terms and thus helps to retain the stability of the scalar potential.

Finally, we argue the primary motivation of this paper. Although the high cutoff scale demands light masses of the extra Higgs bosons, the inverse is not true. Most of the mass spectra in the left panel of Fig. 3 also accommodate a low cutoff scale: see Fig. 1. Even if we observe $m_h = M_A = 100$ GeV and $M_{H^\pm} = 140$ GeV, for example, the mass spectrum alone cannot tell whether the cutoff scale is high or low. A suggestion follows to use t_β as a

discriminator of the cutoff scale. However, measuring large t_β is very challenging at the LHC. The value of t_β governs the fermionic productions (from the top quark decay or gluon fusion via quark loops) and fermionic decays of the extra Higgs bosons because all the Yukawa couplings are inversely proportional to t_β in type-I. This is where the difficulty arises. If t_β is large, like $\gtrsim 10$, the fermionic production of the extra Higgs bosons is highly suppressed. Even though the production of the extra Higgs bosons is feasible through the mediation of gauge bosons like $q\bar{q} \rightarrow Z^* \rightarrow Ah$ and $q\bar{q} \rightarrow W^* \rightarrow H^\pm h/A$ [44, 89–99], the production cross sections do not give information about t_β . Moreover, the fermionic decay parts are insensitive to t_β because of the same dependence of all the Yukawa couplings on t_β . If we cannot measure the exact value of large t_β , it is reasonable to include all the viable parameter points with $t_\beta > 10$ when pursuing a way to discriminate the high and low Λ_{cut} .

IV. TRILINEAR HIGGS COUPLINGS AND THE LHC PHENOMENOLOGY

In this section, we study the trilinear Higgs couplings to measure Λ_{cut} . We consider the following three benchmark points:

$$\begin{aligned}
\text{BP-1:} \quad m_h &= 70 \text{ GeV}, & M_A &= 110 \text{ GeV}, & M_{H^\pm} &= 110 \text{ GeV}, & (14) \\
\text{BP-2:} \quad m_h &= 100 \text{ GeV}, & M_A &= 100 \text{ GeV}, & M_{H^\pm} &= 140 \text{ GeV}, \\
\text{BP-3:} \quad m_h &= 110 \text{ GeV}, & M_A &= 70 \text{ GeV}, & M_{H^\pm} &= 140 \text{ GeV}.
\end{aligned}$$

All three accommodate the cutoff scale from $\Lambda_{\text{cut}} = 1 \text{ TeV}$ to 10^{19} GeV . As discussed in the previous section, we focus on the large t_β limit as

$$\text{Large } t_\beta \text{ case: } t_\beta > 10. \quad (15)$$

For m_{12}^2 , we incorporate all the values that satisfy the constraints in Sec. III.

First, we present the branching ratios of h (left panels), A (middle panels), and H^\pm (right panels) as a function of Λ_{cut} in Fig. 4. The results of BP-1, BP-2, and BP-3 are in the upper, middle, and lower panels, respectively. We include all the viable parameter points. The first noteworthy feature in Fig. 4 is that the dominant decay mode of the extra Higgs boson with the given mass spectra is insensitive to the cutoff scale, even though the two parameters of $t_\beta (> 10)$ and m_{12}^2 are not fixed. The decay of h depends on the hierarchy between m_h and M_A . When $m_h \leq M_A$ as in BP-1 and BP-2, the leading (next-to-leading) decay mode is $h \rightarrow b\bar{b}$ ($h \rightarrow \tau^+\tau^-$). However, if $m_h > M_A$ as in BP-3, the dominant decay mode is $h \rightarrow AZ^*$. The suppressed Yukawa couplings of h by large t_β enhance the bosonic decays modes if kinematically open. The decay of A is primarily determined by the hierarchy between M_A and m_h . For BP-1 and BP-2 with $M_A \leq m_h$, the pseudoscalar A dominantly decays into a pair of b quarks with $\text{Br}(A \rightarrow b\bar{b}) \gtrsim 0.73$. The next-to-leading decay mode of A is into gg . The substantial $\text{Br}(A \rightarrow gg)$ is attributed to the larger loop amplitudes of a pseudoscalar than those of a scalar for the spin-1/2 particle contributions [100]. The third one is $A \rightarrow \tau^+\tau^-$. If $M_A > m_h$, however,

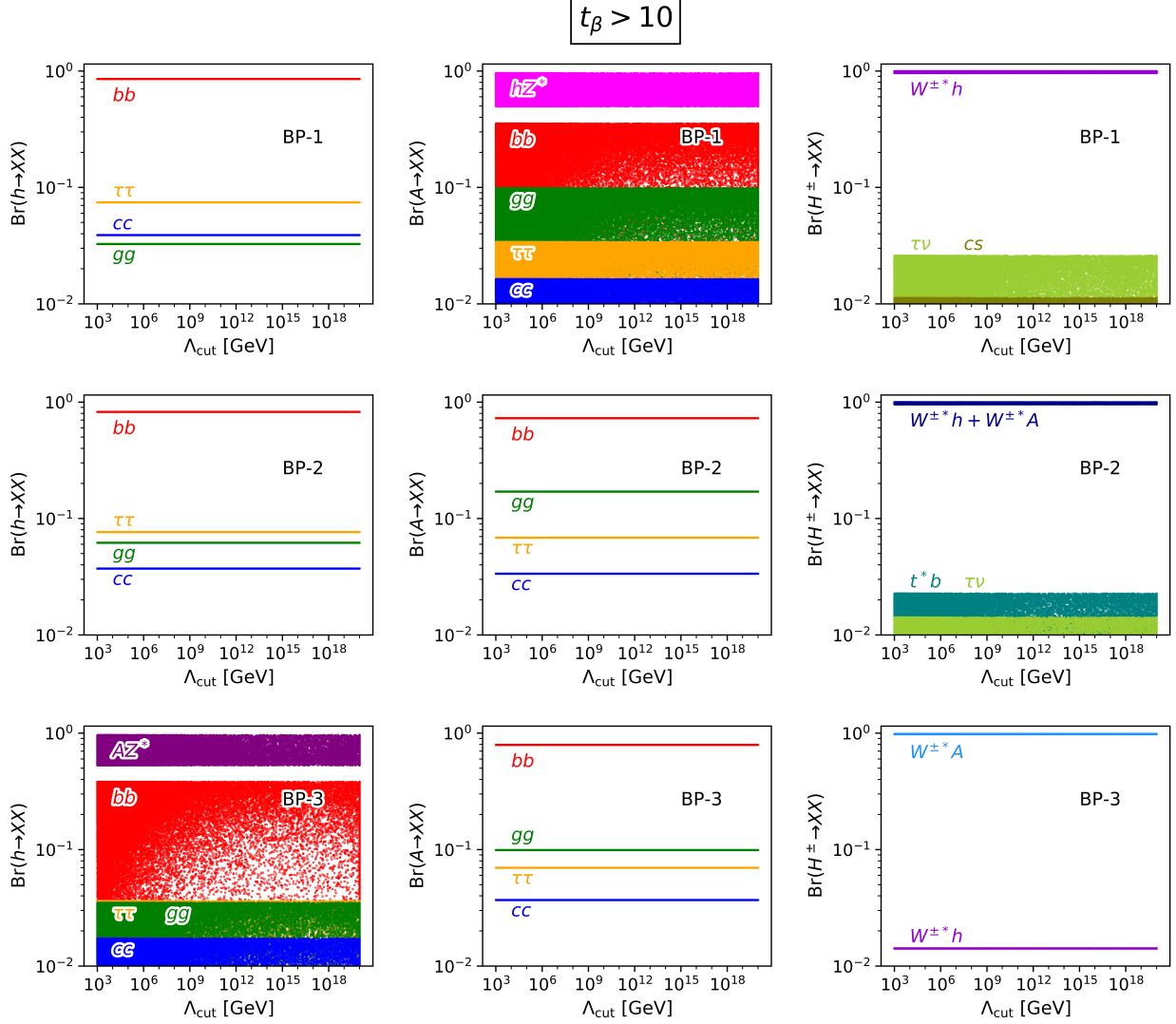


FIG. 4: Branching ratios of h (left panels), A (middle panels), and H^\pm (right panels) for $m_h = M_A = 100$ GeV and $M_{H^\pm} = 140$ GeV, about the cutoff scale Λ_{cut} . All the viable parameter points with $t_\beta > 10$ are included.

$\text{Br}(A \rightarrow hZ^*)$ becomes the largest, which holds for the entire range of Λ_{cut} . The decay into $b\bar{b}$ is mostly next-to-leading.² The branching ratio of $A \rightarrow \tau^+\tau^-$ is similar to that of $A \rightarrow gg$.

The charged Higgs boson mainly decays into $AW^{\pm*}$ and $hW^{\pm*}$, for the three benchmark points. Once kinematically allowed, the bosonic decay modes are leading: the $H^\pm\text{-}W^\mp\text{-}h$ vertex is proportional to $c_{\beta-\alpha}$; the $H^\pm\text{-}W^\mp\text{-}A$ vertex is originated from the pure gauge interaction. In BP-3 with $M_{H^\pm} > M_A$ and $M_{H^\pm} > m_h$, the bosonic decay modes are dominant so that the branching ratios of the fermionic modes are below 1%. If either m_h or M_A is beyond the kinematic threshold as in BP-1 and BP-2, the fermionic decay modes become considerable. The

² We caution the reader that the scattered points are overlapped except for the first dominant decay mode. For some parameter points, therefore, $A \rightarrow gg$ can be next-to-leading.

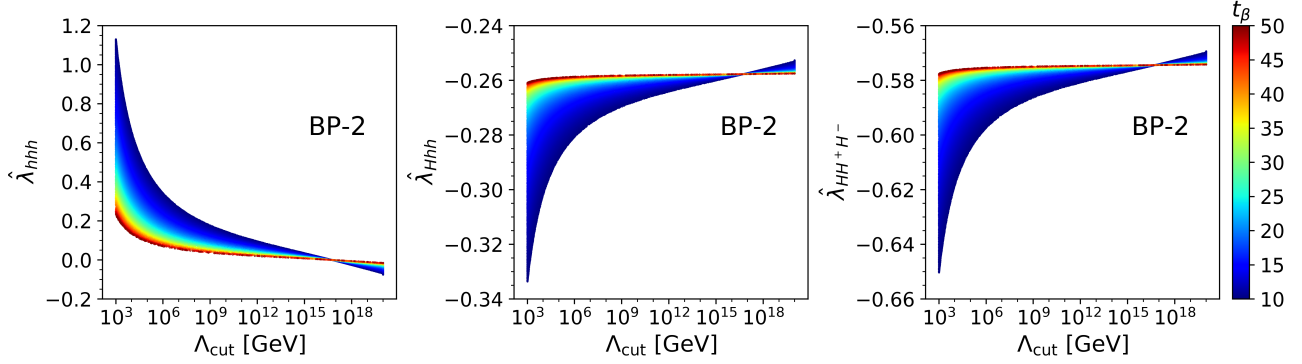


FIG. 5: Trilinear Higgs couplings of $\hat{\lambda}_{hhh}$ (left panel), $\hat{\lambda}_{Hhh}$ (middle panel), and $\hat{\lambda}_{HH+H^-}$ (right panel) against the cutoff scale Λ_{cut} . The color code denotes t_β . We take BP-2 where $m_h = M_A = 100$ GeV, $M_{H^\pm} = 140$ GeV, and $t_\beta > 10$.

leading fermionic decay mode depends delicately on the charged Higgs bosons mass. For BP-1 where M_{H^\pm} is considerably lighter than m_t , $H^\pm \rightarrow \tau\nu$ has the largest branching ratio among the fermionic decay modes, followed by $H^\pm \rightarrow cs$. In BP-2 where M_{H^\pm} is near to m_t , $H^\pm \rightarrow t^*b$ becomes the leading fermionic mode, followed by $H^\pm \rightarrow \tau\nu$.

Let us turn into the trilinear Higgs couplings versus Λ_{cut} . In Fig. 5, we present $\hat{\lambda}_{hhh}$ (left panel), $\hat{\lambda}_{Hhh}$ (middle panel), and $\hat{\lambda}_{HH+H^-}$ (right panel) as a function of Λ_{cut} . Note that $\hat{\lambda}_{hAA} = \hat{\lambda}_{hH+H^-} = \hat{\lambda}_{hhh}/3$. The value of t_β is shown via the color code. Here only the BP-2 results are shown because they are similar to the results of BP-1 and BP-3: the difference is within $\mathcal{O}(10)\%$. It is impressive that the values of $\hat{\lambda}_{hhh}$, $\hat{\lambda}_{Hhh}$, and $\hat{\lambda}_{HH+H^-}$ with $\Lambda_{\text{cut}} = 1$ TeV, although they are spread by the unfixed t_β and m_{12}^2 , are different from those corresponding to $\Lambda_{\text{cut}} \simeq 10^{18}$ GeV. The most sensitive dependence on Λ_{cut} is shown in $\hat{\lambda}_{hhh}$, which ranges in $[-0.09, 1.1]$. Since $\hat{\lambda}_{hhh} = 0$ is included, the change of $\hat{\lambda}_{hhh}$ according to Λ_{cut} is huge. On the other hand, the variations of $\hat{\lambda}_{Hhh}$ and $\hat{\lambda}_{HH+H^-}$ are small within $10\% \sim 20\%$.

Unlike $\hat{\lambda}_{hhh}$, $\hat{\lambda}_{Hhh}$, and $\hat{\lambda}_{HH+H^-}$, the value of $\hat{\lambda}_{HAA}$ is sensitive to the benchmark point. In the left panel of Fig. 6, we present $\hat{\lambda}_{HAA}$ versus Λ_{cut} for the three benchmark points. The large variation of $\hat{\lambda}_{HAA}$ according to the benchmark point is clearly shown: $|\hat{\lambda}_{HAA}|$ of BP-1 is about 25 times larger than that of BP-3 in the high cutoff scale limit. $\hat{\lambda}_{HAA}$ depends on M_A and M^2 , not on t_β . Let us limit the discussion to the high Λ_{cut} case. Since $M^2 \approx m_h$ as shown in Fig. 3 and the M^2 contribution nearly cancels the m_{125} contribution, the effect of M_A on $\hat{\lambda}_{HAA}$ is crucial so that the heavier M_A enhances $\hat{\lambda}_{HAA}$. So, BP-1 with the heaviest M_A has the largest $|\hat{\lambda}_{HAA}|$.

We observe a special Λ_{cut} in Fig. 5 and the right panel of Fig. 6. Around $\Lambda_{\text{cut}} \simeq 10^{17}$ GeV, all the trilinear couplings are almost fixed. Even though we present only the results of BP-2, the same behavior is found in BP-1 and BP-3. The spread trilinear Higgs couplings are focused on a single point which we call $\Lambda_{\text{cut}}^{\text{focus}}$. It corresponds to the parameter points with $M^2 = m_h^2$, which removes the t_β dependence of the trilinear couplings in Eq. (10). Since the variation of $\hat{\lambda}_{\phi\phi'\phi''}$ is originated mainly from the undetermined t_β , the simple condition of $M^2 = m_h^2$ nearly

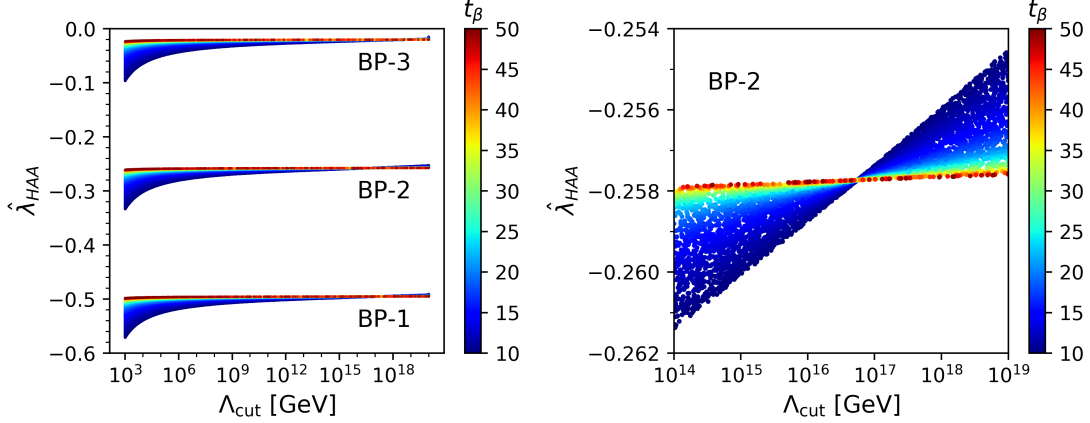


FIG. 6: Trilinear Higgs couplings of $\hat{\lambda}_{HAA}$ versus the cutoff scale Λ_{cut} for BP-1, BP-2, and BP-3 (left panel) and $\hat{\lambda}_{HAA}$ around the *focus* cutoff scale for BP-2 (right panel). The color code denotes t_β . We include all the viable parameter points with $t_\beta > 10$.

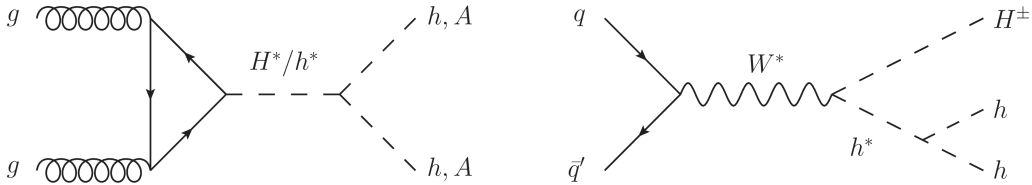


FIG. 7: Feynman diagrams of $gg \rightarrow hh/AA$ (left panel) and $q\bar{q}' \rightarrow W^* \rightarrow H^\pm hh$ (right panel).

fixes the values of $\hat{\lambda}_{\phi\phi'\phi''}$. In particular, $\hat{\lambda}_{hhh}$ vanishes when $\Lambda_{\text{cut}} = \Lambda_{\text{cut}}^{\text{focus}}$.

To probe the trilinear Higgs couplings at the LHC, we need to consider multi-Higgs boson production mediated by Higgs bosons. The first important is the loop-induced process of $gg \rightarrow H/h \rightarrow hh/AA$. The corresponding Feynman diagram is in the left panel of Fig. 7. We omit the box diagrams from the top quark loop because two factors of $1/t_\beta$ suppress them. The contribution of H destructively interferes with that of h because the sign of $\hat{\lambda}_{Hhh}$ and $\hat{\lambda}_{hhh}$ are opposite to each other: see Fig. 5.

In Fig. 8, we present as a function of Λ_{cut} the parton-level production cross sections for $gg \rightarrow hh$ (left panel) and $gg \rightarrow AA$ (right panel) at the 14 TeV LHC over the viable parameter points. All the three benchmark points in Eq. (14) are considered. The color code denotes t_β . To calculate the parton-level cross sections, we first obtained the Universal FeynRules Output (UFO) [101] by using FEYNRULES [102]. Then we interfaced the UFO file with MADGRAPH5-AMC@NLO [103] and calculated the cross sections at the 14 TeV LHC with the NNPDF31_LO_AS_0118 parton distribution function set [104].

For the production cross sections of $gg \rightarrow hh$, the most crucial factor is m_h . The lighter m_h is, the larger $\sigma(gg \rightarrow hh)$ is. So, BP-1 yields the largest cross section. On the contrary, the production cross section of $gg \rightarrow AA$ is larger for heavier M_A . The BP-1, which has the heaviest M_A among the three benchmark points, has the largest cross section. It seems contradictory

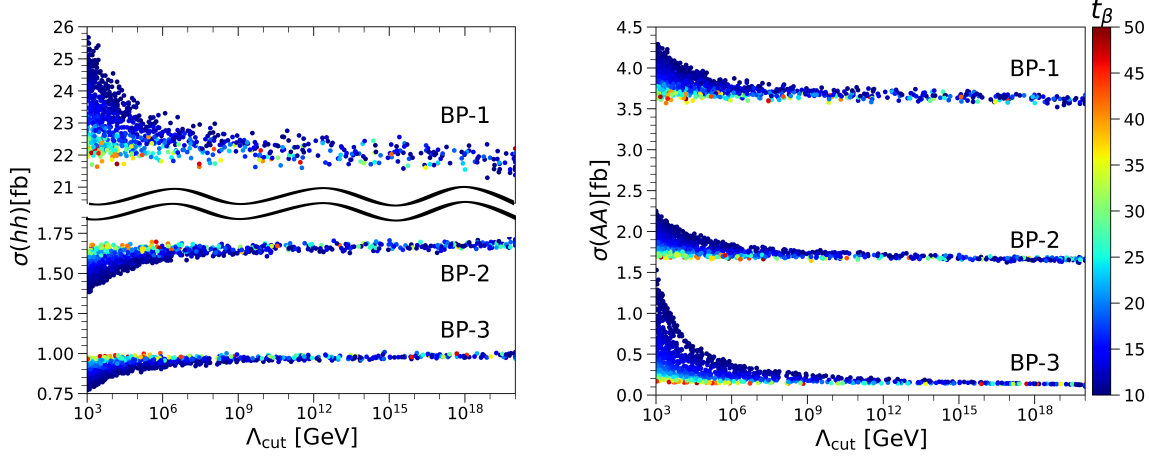


FIG. 8: Cross sections of $gg \rightarrow hh$ (left panel) and $gg \rightarrow AA$ (right panel) at the 14 TeV LHC, as a function of Λ_{cut} . The color code denotes t_β . The description of the benchmarks are in the main text.

to the kinematic loss by the heavy M_A . The main reason is that the dominant contribution to $gg \rightarrow AA$ is from H and thus $\hat{\lambda}_{HAA}$ governs the process. As shown in Fig. 6, $\hat{\lambda}_{HAA}$ is much larger for a heavy M_A .

The dependence of $\sigma(gg \rightarrow hh/AA)$ on Λ_{cut} is not large enough to distinct the high and low cutoff scales. Even the optimistic case, the process of $gg \rightarrow hh$ in BP-1 with $t_\beta = 10$, makes a few fb difference in the cross sections between $\Lambda_{\text{cut}} = 1$ TeV and $\Lambda_{\text{cut}} = 10^{18}$ GeV. It is too small to probe at the HL-LHC with the expected total luminosity of 3 ab^{-1} . For larger t_β , the di-Higgs production cross sections become more insensitive to Λ_{cut} . The weak dependence of $\sigma(gg \rightarrow hh)$ on Λ_{cut} is due to the *dominant* contribution from H and the *destructive* interference between the H and h contributions. Let us consider BP-1 with $t_\beta = 10$ and $\Lambda_{\text{cut}} = 1$ TeV. The cross section from H alone is $\sigma(gg \rightarrow H \rightarrow hh) \simeq 36.5$ fb, from h alone is $\sigma(gg \rightarrow h \rightarrow hh) \simeq 1.1$ fb, and from the interference alone $\sigma(gg \rightarrow hh)_{\text{intf}} \simeq -12.1$ fb. The $\hat{\lambda}_{Hhh}$ controls the cross section, but its variation about Λ_{cut} is small.

To single out only one trilinear Higgs coupling, we consider triple Higgs production at the LHC. Since the gluon fusion production of the tri-Higgs process through the top quark loop is suppressed by large t_β , the efficient tri-Higgs productions are the ones mediated by the gauge bosons. Through the Z boson, we have

$$q\bar{q} \rightarrow Z^* \rightarrow Ah^* \rightarrow Ahh, \quad q\bar{q} \rightarrow Z^* \rightarrow A^*h \rightarrow Ahh, \quad (16)$$

$$q\bar{q} \rightarrow Z^* \rightarrow Ah^* \rightarrow AAA, \quad (17)$$

and through W

$$q\bar{q}' \rightarrow W^* \rightarrow H^\pm h^* \rightarrow H^\pm hh, \quad (18)$$

$$q\bar{q}' \rightarrow W^* \rightarrow H^\pm h^* \rightarrow H^\pm AA, \quad (19)$$

$$q\bar{q}' \rightarrow W^* \rightarrow H^\pm A^* \rightarrow H^\pm Ah. \quad (20)$$

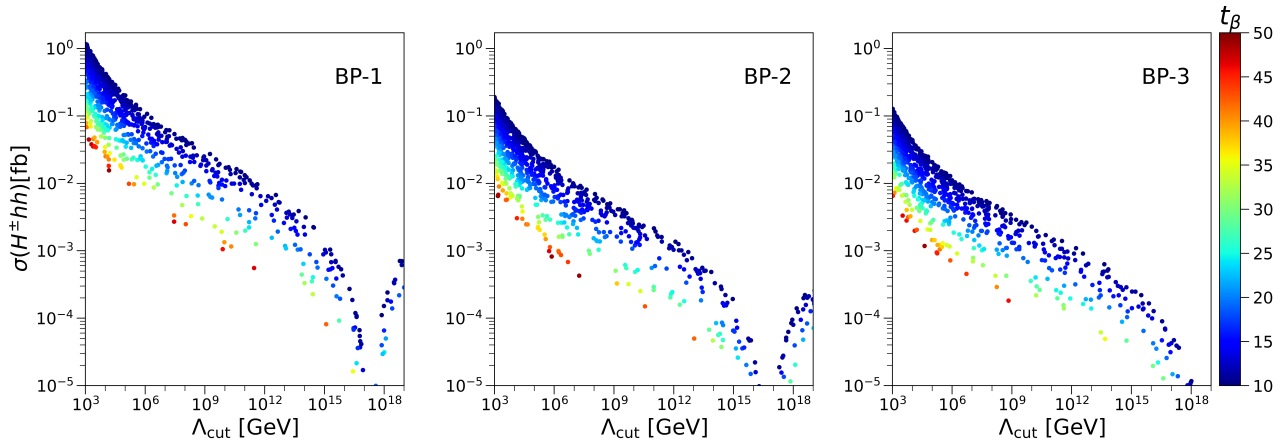


FIG. 9: Cross sections of $q\bar{q}' \rightarrow H^\pm hh$ at the 14 TeV LHC as a function of Λ_{cut} , for BP-1 (left), BP-2 (middle), and BP-3 (right). The color codes indicate t_β .

As a representative, we present the Feynman diagram of $q\bar{q}' \rightarrow H^\pm hh$ in the right panel of Fig. 7. Since all the above processes have the same topology of the Feynman diagram, the production cross sections as a function of Λ_{cut} show almost the same behavior. For example, $\sigma(pp \rightarrow Ahh)/\sigma(pp \rightarrow H^\pm hh) \simeq 0.9$ holds for all Λ_{cut} in BP-2.

In Fig. 9, we present the parton-level production cross sections of $q\bar{q}' \rightarrow H^\pm hh$ at the 14 TeV LHC for BP-1 (left panel), BP-2 (middle panel), and BP-3 (right panel). The color code denotes t_β . The most significant result in Fig. 9 is that the difference of the cross section according to Λ_{cut} is big enough to distinguish the high and low cutoff scales of the inverted type-I. The ratio of the cross section for $\Lambda_{\text{cut}} = 1$ TeV to that for $\Lambda_{\text{cut}} = 10^{18}$ GeV is more than about 10^3 . This is the most remarkable result of our study. Measuring the signal rate of the triple Higgs production tells whether the cutoff scale is high or low.

Finally, we discuss the discovery potential at the HL-LHC. Discriminating the high and low cutoff scales through $gg \rightarrow hh/AA$ requires the precision measurement on the cross section within ~ 1 fb. Let us roughly estimate the feasibility. The processes of $gg \rightarrow hh$ and $gg \rightarrow AA$ mainly yield $4b$ final states because $A/h \rightarrow bb$ is leading or next-to-leading. Resembling the di-Higgs process in the SM, they are challenging to observe for two reasons. First, the cross sections are too small. The maximum of the cross section, which happens for $\Lambda_{\text{cut}} = 1$ TeV, reaches $\mathcal{O}(10)$ fb. It is to be compared with the SM leading order result of $\sigma(gg \rightarrow h_{\text{SM}} h_{\text{SM}})_{\text{LO}} \simeq 17$ fb at $\sqrt{s} = 14$ TeV [105]. The projected signal significance at the HL-LHC with the total luminosity of 3 ab^{-1} is 3.0σ , when the $bbbb$, $bb\tau^+\tau^-$, and $bb\gamma\gamma$ decay channels are all combined [106]. The second difficulty comes from the softer b jets than in the SM di-Higgs process, which reduces the b tagging efficiency. For $gg \rightarrow hh \rightarrow 4b$, the lighter m_h than 125 GeV always yields soft b quarks. For $gg \rightarrow AA \rightarrow 4b$, most of the viable parameter points in Fig. 3 have $M_A < 125$ GeV, which generate soft b quarks. In summary, the di-Higgs process is not efficient to probe the cutoff scale.

The triple Higgs production of $H^\pm hh$, $H^\pm AA$, and $H^\pm Ah$ in Eqs. (18)–(20), mediated by

the W boson, has higher discovery potential. If the charged Higgs boson mainly decays into $W^{\pm*}A/h$ as in the three benchmark points, followed by $h/A \rightarrow bb$, the final state is $6b + \ell\nu$. This attractive channel has not been studied in the literature.³ The main backgrounds are

$$\begin{aligned} t + \bar{t} + \ell\nu &\rightarrow b j_b^{\text{mis}} j_b^{\text{mis}} + b j_b^{\text{mis}} j_b^{\text{mis}} + \ell\nu, \\ t + \bar{t} + jj &\rightarrow b\ell\nu + b j_b^{\text{mis}} j_b^{\text{mis}} + j_b^{\text{mis}} j_b^{\text{mis}}, \end{aligned} \quad (21)$$

where j_b^{mis} is the light jet (from $u, d, s, c,$ and g) mistagged as a b quark jet. We calculated the parton-level cross sections of $t\bar{t} + \ell\nu$ and $t\bar{t} + bb$, with the b tagging and mistagging efficiencies of $P_{b \rightarrow b} = 0.7$, $P_{c \rightarrow b} = 0.05$, and $P_{j \rightarrow b} = 0.01$. We imposed the selection cuts of $p_T^b > 20$ GeV, $p_T^\ell > 10$ GeV, $|\eta^{\ell,j}| < 2.5$, $E_T^{\text{miss}} > 20$ GeV, and the separation $\Delta R_{i'j'} > 0.4$. After the basic selection, the background cross section from $t\bar{t} + bb$ is about 8.7 ab and that from $t\bar{t} + \ell\nu$ is 3.8×10^{-4} ab. If we impose additional cuts on the invariant mass of two b jets like $|m_{bb} - m_h| < 15$ GeV, the backgrounds are negligible. Despite the almost background-free environment, the high Λ_{cut} yields too small signal rate of $pp \rightarrow H^\pm hh$ at the 14 TeV LHC.

Exploring the cutoff scale in the inverted type-I via the $6b + \ell\nu$ final state has a better chance in future high-energy colliders such as the Future hadron-hadron Circular Collider (FCC-hh) at CERN [109], the CEPC [110, 111], and the muon collider [112–114]. We have particular expectations for the muon collider with benchmark energies in the range of $\sqrt{s} = 3 - 30$ TeV and the integrated luminosity of $\mathcal{L} = 10(\sqrt{s}/10 \text{ TeV})^2 \text{ ab}^{-1}$. The triple Higgs processes in Eq. (16) and Eq. (17) with $q\bar{q}$ replaced by $\mu^+\mu^-$ will be very helpful to disentangle the high and low cutoff scales of the inverted type-I.

V. CONCLUSION

Beyond the studies on how high the cutoff scale of a new physics model can go up, we have pursued an efficient observable to distinguish the high and low cutoff scales. The type-I in the 2HDM has been considered for the inverted scenario where the observed Higgs boson at a mass of 125 GeV is the heavier CP -even Higgs boson H . We have first obtained the still-available parameter points that satisfy the theoretical requirements, the experimental constraints, and the cutoff scale above 1 TeV. The viable parameter space at the electroweak scale is already limited such that $M_A, M_{H^\pm} \lesssim 430$ GeV and $m_h \gtrsim 62.5$ GeV. Through the calculation of the cutoff scale Λ_{cut} of each viable parameter point by using the RGE, we have shown that the inverted type-I can retain the stability all the way up to the Planck scale.

The condition of $\Lambda_{\text{cut}} > 10^{18}$ GeV requires the light masses of the extra Higgs bosons like $M_A, M_{H^\pm} \lesssim 160$ GeV. However, the light masses alone cannot guarantee the high cutoff scale because the parameter points with light masses accommodate Λ_{cut} from 1 TeV to 10^{19} GeV. Targeting at the phenomenologically challenging case of $t_\beta > 10$, we have investigated the

³ The final state of $4j + \ell\nu$ was studied for the vector boson scattering of $WW \rightarrow WW$ [107], and the SM Higgs boson decaying into a fat jet consisting of $4b/6b/8b$ was studied [108].

trilinear Higgs couplings, $\hat{\lambda}_{\phi\phi'\phi''}$, versus Λ_{cut} . Although the values of all the $\hat{\lambda}_{\phi\phi'\phi''}$ at $\Lambda_{\text{cut}} = 1$ TeV are different from those at $\Lambda_{\text{cut}} = 10^{18}$ GeV, only the $\hat{\lambda}_{hhh}$ shows a large variation about Λ_{cut} , $\hat{\lambda}_{hhh} \in [-0.09, 1.1]$. Multi-Higgs boson productions at the LHC have been studied to probe the cutoff scale via $\hat{\lambda}_{\phi\phi'\phi''}$. The gluon fusion productions of the di-Higgs, $gg \rightarrow hh/AA$, are not efficient to measure $\hat{\lambda}_{hhh}$ because the dominant contribution from H dilutes the h contribution. The most remarkable result is in the tri-Higgs process of $pp \rightarrow H^\pm hh$ mediated by the W boson. The signal cross section shows huge variation according to Λ_{cut} , $\sigma_{\Lambda_{\text{cut}}=1 \text{ TeV}}/\sigma_{\Lambda_{\text{cut}}=10^{18} \text{ GeV}} \gtrsim 10^3$. The precision measurement of $pp \rightarrow H^\pm hh$ can indeed distinguish the high and low cutoff scales of the model. Considering the dominant decay modes of $H^\pm \rightarrow W^{\pm*}A/h$, $h \rightarrow bb$, and $A \rightarrow bb$, the final state of $pp \rightarrow H^\pm hh$ is $6b+\ell\nu$. Although it enjoys almost background free environment at the LHC, the small cross section ($\lesssim 1$ ab) for $\Lambda_{\text{cut}} = 10^{18}$ GeV motivates future high-energy colliders, especially the muon collider with $\sqrt{s} = 3 - 30$ TeV.

Acknowledgments

The work of JK, SL, and JS is supported by the National Research Foundation of Korea, Grant No. NRF-2022R1A2C1007583.

Appendix A: RGEs in the type-I 2HDM

Focusing on the type-I 2HDM, we present the one-loop level RGEs [30, 38, 45, 115, 116]. The beta functions of gauge couplings are given by

$$16\pi^2\beta_{g_3} = -7g_3^3, \quad (\text{A1})$$

$$16\pi^2\beta_{g_2} = \left(-\frac{10}{3} + \frac{n_d}{6}\right)g_2^3 = -3g_2^3, \quad (\text{A2})$$

$$16\pi^2\beta_{g_1} = \left(\frac{20}{3} + \frac{n_d}{6}\right)g_1^3, \quad (\text{A3})$$

where n_d is the number of the scalar doublets of the fermions, so $n_d = 2$ in the 2HDM. The running of the quartic couplings of λ_i 's is different according to the type. First, we write the β functions in terms of the common part c_i and the type-dependent part h_i as

$$16\pi^2\beta_{\lambda_i}^{\text{type}} = c_i + h_i^{\text{type}}, \quad (i = 1, \dots, 5). \quad (\text{A4})$$

The common parts for λ_i 's are

$$c_1 = 12\lambda_1^2 + 4\lambda_3^2 + 4\lambda_3\lambda_4 + 2\lambda_4^2 + 2\lambda_5^2 + \frac{3}{4}(3g^4 + g'^4 + 2g^2g'^2) - 3\lambda_1(3g^2 + g'^2), \quad (\text{A5})$$

$$c_2 = 12\lambda_2^2 + 4\lambda_3^2 + 4\lambda_3\lambda_4 + 2\lambda_4^2 + 2\lambda_5^2 + \frac{3}{4}(3g^4 + g'^4 + 2g^2g'^2) - 3\lambda_2(3g^2 + g'^2) \\ + 12y_t^2\lambda_2 - 12y_t^4,$$

$$c_3 = (\lambda_1 + \lambda_2)(6\lambda_3 + 2\lambda_4) + 4\lambda_3^2 + 2\lambda_4^2 + 2\lambda_5^2 + \frac{3}{4}(3g^4 + g'^4 - 2g^2g'^2) - 3\lambda_3(3g^2 + g'^2) \\ + 2(3y_t^2 + 3y_b^2 + y_\tau^2)\lambda_3,$$

$$c_4 = 2(\lambda_1 + \lambda_2)\lambda_4 + 8\lambda_3\lambda_4 + 4\lambda_4^2 + 8\lambda_5^2 + 3g^2g'^2 - 3(3g^2 + g'^2)\lambda_4 \\ + 2(3y_t^2 + 3y_b^2 + y_\tau^2)\lambda_4,$$

$$c_5 = 2(\lambda_1 + \lambda_2 + 4\lambda_3 + 6\lambda_4)\lambda_5 - 3\lambda_5(3g^2 + g'^2) + 2(3y_t^2 + 3y_b^2 + y_\tau^2)\lambda_5.$$

The h_i 's in type-I are

$$h_1^I = h_3^I = h_4^I = h_5^I = 0, \quad (\text{A6})$$

$$h_2^I = 4(3y_b^2 + y_\tau^2)\lambda_2 - 4(3y_b^4 + y_\tau^4).$$

The Yukawa couplings of the top quark, bottom quark, and tau lepton (y_t , y_b , and y_τ) are running with the β functions of

$$16\pi^2\beta_{y_f}^{\text{type}} = c_{y_f} + h_{y_f}^{\text{type}}, \quad (f = t, b, \tau), \quad (\text{A7})$$

where the common parts are

$$c_{y_t} = \left(-8g_s^2 - \frac{9}{4}g^2 - \frac{17}{12}g'^2 + \frac{9}{2}y_t^2 \right) y_t, \quad (\text{A8})$$

$$c_{y_b} = \left(-8g_s^2 - \frac{9}{4}g^2 - \frac{5}{12}g'^2 + \frac{3}{2}y_t^2 + \frac{9}{2}y_b^2 \right) y_b, \quad (\text{A9})$$

$$c_{y_\tau} = \left(-\frac{9}{4}g^2 - \frac{15}{4}g'^2 + \frac{5}{2}y_\tau^2 \right) y_\tau,$$

and the type-dependent parts are

$$h_{y_t}^I = \left(\frac{3}{2}y_b^2 + y_\tau^2 \right) y_t, \quad h_{y_b}^I = y_\tau^2 y_b, \quad h_{y_\tau}^I = 3(y_t^2 + y_b^2) y_\tau. \quad (\text{A10})$$

The initial conditions of the Yukawa coupling are set at the top quark mass scale m_t^{pole} [30] as

$$y_t(m_t^{\text{pole}}) = \frac{\sqrt{2}m_t}{v s_\beta} \left\{ 1 - \frac{4}{3\pi}\alpha_s(m_t) \right\}, \quad (\text{A11})$$

$$y_b(m_t^{\text{pole}}) = \frac{\sqrt{2}m_b}{v s_\beta},$$

$$y_\tau(m_t^{\text{pole}}) = \frac{\sqrt{2}m_\tau}{v s_\beta}.$$

-
- [1] J. Ellis, *SMEFT Constraints on New Physics beyond the Standard Model*, in *Beyond Standard Model: From Theory to Experiment*, 5, 2021. [2105.14942](#). DOI.
- [2] ATLAS collaboration, G. Aad et al., *Measurements of WH and ZH production in the $H \rightarrow b\bar{b}$ decay channel in pp collisions at 13 TeV with the ATLAS detector*, *Eur. Phys. J. C* **81** (2021) 178, [[2007.02873](#)].
- [3] ATLAS collaboration, G. Aad et al., *Measurements of Higgs bosons decaying to bottom quarks from vector boson fusion production with the ATLAS experiment at $\sqrt{s} = 13$ TeV*, *Eur. Phys. J. C* **81** (2021) 537, [[2011.08280](#)].
- [4] CMS collaboration, A. M. Sirunyan et al., *Inclusive search for highly boosted Higgs bosons decaying to bottom quark-antiquark pairs in proton-proton collisions at $\sqrt{s} = 13$ TeV*, *JHEP* **12** (2020) 085, [[2006.13251](#)].
- [5] ATLAS collaboration, *Study of Higgs-boson production with large transverse momentum using the $H \rightarrow b\bar{b}$ decay with the ATLAS detector*, .
- [6] CMS collaboration, A. Tumasyan et al., *Measurement of the inclusive and differential Higgs boson production cross sections in the decay mode to a pair of τ leptons in pp collisions at $\sqrt{s} = 13$ TeV*, *Phys. Rev. Lett.* **128** (2022) 081805, [[2107.11486](#)].
- [7] ATLAS collaboration, *Measurement of the Higgs boson decaying to b -quarks produced in association with a top-quark pair in pp collisions at $\sqrt{s} = 13$ TeV with the ATLAS detector*, .
- [8] ATLAS collaboration, *Measurements of gluon fusion and vector-boson-fusion production of the Higgs boson in $H \rightarrow WW^* \rightarrow e\nu\mu\nu$ decays using pp collisions at $\sqrt{s} = 13$ TeV with the ATLAS detector*, .
- [9] ATLAS collaboration, *Measurement of the properties of Higgs boson production at $\sqrt{s}=13$ TeV in the $H \rightarrow \gamma\gamma$ channel using 139 fb^{-1} of pp collision data with the ATLAS experiment*, .
- [10] CMS collaboration, A. M. Sirunyan et al., *Measurements of production cross sections of the Higgs boson in the four-lepton final state in proton-proton collisions at $\sqrt{s} = 13$ TeV*, *Eur. Phys. J. C* **81** (2021) 488, [[2103.04956](#)].
- [11] ATLAS collaboration, G. Aad et al., *Measurements of the Higgs boson inclusive and differential fiducial cross sections in the 4ℓ decay channel at $\sqrt{s} = 13$ TeV*, *Eur. Phys. J. C* **80** (2020) 942, [[2004.03969](#)].
- [12] ATLAS collaboration, G. Aad et al., *Higgs boson production cross-section measurements and their EFT interpretation in the 4ℓ decay channel at $\sqrt{s} = 13$ TeV with the ATLAS detector*, *Eur. Phys. J. C* **80** (2020) 957, [[2004.03447](#)].
- [13] ATLAS collaboration, *A combination of measurements of Higgs boson production and decay using up to 139 fb^{-1} of proton-proton collision data at $\sqrt{s} = 13$ TeV collected with the ATLAS experiment*, .
- [14] ATLAS collaboration, G. Aad et al., *A search for the dimuon decay of the Standard Model Higgs boson with the ATLAS detector*, *Phys. Lett. B* **812** (2021) 135980, [[2007.07830](#)].

- [15] CMS collaboration, A. M. Sirunyan et al., *Evidence for Higgs boson decay to a pair of muons*, *JHEP* **01** (2021) 148, [2009.04363].
- [16] ATLAS collaboration, *Direct constraint on the Higgs-charm coupling from a search for Higgs boson decays to charm quarks with the ATLAS detector*, .
- [17] I. Brivio and M. Trott, *Scheming in the SMEFT... and a reparameterization invariance!*, *JHEP* **07** (2017) 148, [1701.06424].
- [18] J. Ellis, C. W. Murphy, V. Sanz and T. You, *Updated Global SMEFT Fit to Higgs, Diboson and Electroweak Data*, *JHEP* **06** (2018) 146, [1803.03252].
- [19] S. Dawson, S. Homiller and S. D. Lane, *Putting standard model EFT fits to work*, *Phys. Rev. D* **102** (2020) 055012, [2007.01296].
- [20] SMEFT collaboration, J. J. Ethier, G. Magni, F. Maltoni, L. Mantani, E. R. Nocera, J. Rojo et al., *Combined SMEFT interpretation of Higgs, diboson, and top quark data from the LHC*, *JHEP* **11** (2021) 089, [2105.00006].
- [21] N. Turok and J. Zadrozny, *Electroweak baryogenesis in the two doublet model*, *Nucl. Phys. B* **358** (1991) 471–493.
- [22] A. G. Cohen, D. B. Kaplan and A. E. Nelson, *Spontaneous baryogenesis at the weak phase transition*, *Phys. Lett. B* **263** (1991) 86–92.
- [23] V. Zarikas, *The Phase transition of the two Higgs extension of the standard model*, *Phys. Lett. B* **384** (1996) 180–184, [hep-ph/9509338].
- [24] J. M. Cline and P.-A. Lemieux, *Electroweak phase transition in two Higgs doublet models*, *Phys. Rev. D* **55** (1997) 3873–3881, [hep-ph/9609240].
- [25] L. Fromme, S. J. Huber and M. Seniuch, *Baryogenesis in the two-Higgs doublet model*, *JHEP* **11** (2006) 038, [hep-ph/0605242].
- [26] M. E. Machacek and M. T. Vaughn, *Two Loop Renormalization Group Equations in a General Quantum Field Theory. 1. Wave Function Renormalization*, *Nucl. Phys. B* **222** (1983) 83–103.
- [27] M. E. Machacek and M. T. Vaughn, *Two Loop Renormalization Group Equations in a General Quantum Field Theory. 2. Yukawa Couplings*, *Nucl. Phys. B* **236** (1984) 221–232.
- [28] M. E. Machacek and M. T. Vaughn, *Two Loop Renormalization Group Equations in a General Quantum Field Theory. 3. Scalar Quartic Couplings*, *Nucl. Phys. B* **249** (1985) 70–92.
- [29] M.-x. Luo, H.-w. Wang and Y. Xiao, *Two loop renormalization group equations in general gauge field theories*, *Phys. Rev. D* **67** (2003) 065019, [hep-ph/0211440].
- [30] D. Das and I. Saha, *Search for a stable alignment limit in two-Higgs-doublet models*, *Phys. Rev. D* **91** (2015) 095024, [1503.02135].
- [31] H. E. Haber and R. Hempfling, *The Renormalization group improved Higgs sector of the minimal supersymmetric model*, *Phys. Rev. D* **48** (1993) 4280–4309, [hep-ph/9307201].
- [32] W. Grimus and L. Lavoura, *Renormalization of the neutrino mass operators in the multi-Higgs-doublet standard model*, *Eur. Phys. J. C* **39** (2005) 219–227, [hep-ph/0409231].
- [33] P. M. Ferreira, R. Santos, M. Sher and J. P. Silva, *Could the LHC two-photon signal correspond to the heavier scalar in two-Higgs-doublet models?*, *Phys. Rev. D* **85** (2012)

- 035020, [1201.0019].
- [34] S. Chang, S. K. Kang, J.-P. Lee and J. Song, *Higgs potential and hidden light Higgs scenario in two Higgs doublet models*, *Phys. Rev. D* **92** (2015) 075023, [1507.03618].
- [35] A. Jueid, J. Kim, S. Lee and J. Song, *Type- X two-Higgs-doublet model in light of the muon $g-2$: Confronting Higgs boson and collider data*, *Phys. Rev. D* **104** (2021) 095008, [2104.10175].
- [36] S. Lee, K. Cheung, J. Kim, C.-T. Lu and J. Song, *Status of the two-Higgs-doublet model in light of the CDF m_W measurement*, 2204.10338.
- [37] D. Chowdhury and O. Eberhardt, *Global fits of the two-loop renormalized Two-Higgs-Doublet model with soft Z_2 breaking*, *JHEP* **11** (2015) 052, [1503.08216].
- [38] P. Basler, P. M. Ferreira, M. Mühlleitner and R. Santos, *High scale impact in alignment and decoupling in two-Higgs doublet models*, *Phys. Rev. D* **97** (2018) 095024, [1710.10410].
- [39] M. E. Krauss, T. Opferkuch and F. Staub, *The Ultraviolet Landscape of Two-Higgs Doublet Models*, *Eur. Phys. J. C* **78** (2018) 1020, [1807.07581].
- [40] J. Oredsson and J. Rathsmann, *Z_2 breaking effects in 2-loop RG evolution of 2HDM*, *JHEP* **02** (2019) 152, [1810.02588].
- [41] M. Aiko and S. Kanemura, *New scenario for aligned Higgs couplings originated from the twisted custodial symmetry at high energies*, *JHEP* **02** (2021) 046, [2009.04330].
- [42] A. Dey, J. Lahiri and B. Mukhopadhyaya, *Muon $\langle \mathcal{M} \rangle g \langle \mathcal{M} \rangle^{-2}$ and a type- X two-Higgs-doublet scenario: Some studies in high-scale validity*, *Phys. Rev. D* **106** (2022) 055023, [2106.01449].
- [43] J. Kim, S. Lee, P. Sanyal and J. Song, *CDF W -boson mass and muon $g-2$ in a type- X two-Higgs-doublet model with a Higgs-phobic light pseudoscalar*, *Phys. Rev. D* **106** (2022) 035002, [2205.01701].
- [44] J. Kim, S. Lee, J. Song and P. Sanyal, *Fermiophobic light Higgs boson in the type- I two-Higgs-doublet model*, *Phys. Lett. B* **834** (2022) 137406, [2207.05104].
- [45] G. C. Branco, P. M. Ferreira, L. Lavoura, M. N. Rebelo, M. Sher and J. P. Silva, *Theory and phenomenology of two-Higgs-doublet models*, *Phys. Rept.* **516** (2012) 1–102, [1106.0034].
- [46] S. L. Glashow and S. Weinberg, *Natural Conservation Laws for Neutral Currents*, *Phys. Rev. D* **15** (1977) 1958.
- [47] E. A. Paschos, *Diagonal Neutral Currents*, *Phys. Rev. D* **15** (1977) 1966.
- [48] H. E. Haber and D. O’Neil, *Basis-independent methods for the two-Higgs-doublet model. II. The Significance of $\tan\beta$* , *Phys. Rev. D* **74** (2006) 015018, [hep-ph/0602242].
- [49] J. Song and Y. W. Yoon, *$W\gamma$ decay of the elusive charged Higgs boson in the two-Higgs-doublet model with vectorlike fermions*, *Phys. Rev. D* **100** (2019) 055006, [1904.06521].
- [50] S. Kanemura, Y. Okada, H. Taniguchi and K. Tsumura, *Indirect bounds on heavy scalar masses of the two-Higgs-doublet model in light of recent Higgs boson searches*, *Phys. Lett. B* **704** (2011) 303–307, [1108.3297].
- [51] I. P. Ivanov, *Minkowski space structure of the Higgs potential in 2HDM*, *Phys. Rev. D* **75**

- (2007) 035001, [[hep-ph/0609018](#)].
- [52] A. Arhrib, *Unitarity constraints on scalar parameters of the standard and two Higgs doublets model*, in *Workshop on Noncommutative Geometry, Superstrings and Particle Physics*, 12, 2000. [hep-ph/0012353](#).
- [53] I. P. Ivanov, *General two-order-parameter Ginzburg-Landau model with quadratic and quartic interactions*, *Phys. Rev. E* **79** (2009) 021116, [[0802.2107](#)].
- [54] A. Barroso, P. M. Ferreira, I. P. Ivanov, R. Santos and J. P. Silva, *Evading death by vacuum*, *Eur. Phys. J. C* **73** (2013) 2537, [[1211.6119](#)].
- [55] A. Barroso, P. M. Ferreira, I. P. Ivanov and R. Santos, *Metastability bounds on the two Higgs doublet model*, *JHEP* **06** (2013) 045, [[1303.5098](#)].
- [56] M. E. Peskin and T. Takeuchi, *Estimation of oblique electroweak corrections*, *Phys. Rev. D* **46** (1992) 381–409.
- [57] H.-J. He, N. Polonsky and S.-f. Su, *Extra families, Higgs spectrum and oblique corrections*, *Phys. Rev. D* **64** (2001) 053004, [[hep-ph/0102144](#)].
- [58] W. Grimus, L. Lavoura, O. M. Ogreid and P. Osland, *The Oblique parameters in multi-Higgs-doublet models*, *Nucl. Phys. B* **801** (2008) 81–96, [[0802.4353](#)].
- [59] PARTICLE DATA GROUP collaboration, P. A. Zyla et al., *Review of Particle Physics*, *PTEP* **2020** (2020) 083C01.
- [60] A. Arbey, F. Mahmoudi, O. Stal and T. Stefaniak, *Status of the Charged Higgs Boson in Two Higgs Doublet Models*, *Eur. Phys. J. C* **78** (2018) 182, [[1706.07414](#)].
- [61] P. Sanyal, *Limits on the Charged Higgs Parameters in the Two Higgs Doublet Model using CMS $\sqrt{s} = 13$ TeV Results*, *Eur. Phys. J. C* **79** (2019) 913, [[1906.02520](#)].
- [62] M. Misiak and M. Steinhauser, *Weak radiative decays of the B meson and bounds on M_{H^\pm} in the Two-Higgs-Doublet Model*, *Eur. Phys. J. C* **77** (2017) 201, [[1702.04571](#)].
- [63] P. Bechtle, S. Heinemeyer, T. Klingl, T. Stefaniak, G. Weiglein and J. Wittbrodt, *HiggsSignals-2: Probing new physics with precision Higgs measurements in the LHC 13 TeV era*, *Eur. Phys. J. C* **81** (2021) 145, [[2012.09197](#)].
- [64] ATLAS collaboration, M. Aaboud et al., *Search for Higgs bosons produced via vector-boson fusion and decaying into bottom quark pairs in $\sqrt{s} = 13$ TeV pp collisions with the ATLAS detector*, *Phys. Rev. D* **98** (2018) 052003, [[1807.08639](#)].
- [65] ATLAS collaboration, M. Aaboud et al., *Measurements of gluon-gluon fusion and vector-boson fusion Higgs boson production cross-sections in the $H \rightarrow WW^* \rightarrow e\nu\mu\nu$ decay channel in pp collisions at $\sqrt{s} = 13$ TeV with the ATLAS detector*, *Phys. Lett. B* **789** (2019) 508–529, [[1808.09054](#)].
- [66] ATLAS collaboration, M. Aaboud et al., *Cross-section measurements of the Higgs boson decaying into a pair of τ -leptons in proton-proton collisions at $\sqrt{s} = 13$ TeV with the ATLAS detector*, *Phys. Rev. D* **99** (2019) 072001, [[1811.08856](#)].
- [67] ATLAS collaboration, G. Aad et al., *Higgs boson production cross-section measurements and their EFT interpretation in the 4ℓ decay channel at $\sqrt{s} = 13$ TeV with the ATLAS detector*,

- Eur. Phys. J. C* **80** (2020) 957, [2004.03447].
- [68] CMS collaboration, A. M. Sirunyan et al., *Search for $t\bar{t}H$ production in the $H \rightarrow b\bar{b}$ decay channel with leptonic $t\bar{t}$ decays in proton-proton collisions at $\sqrt{s} = 13$ TeV*, *JHEP* **03** (2019) 026, [1804.03682].
- [69] CMS collaboration, A. M. Sirunyan et al., *Search for the Higgs boson decaying to two muons in proton-proton collisions at $\sqrt{s} = 13$ TeV*, *Phys. Rev. Lett.* **122** (2019) 021801, [1807.06325].
- [70] CMS collaboration, *Measurements of properties of the Higgs boson in the four-lepton final state in proton-proton collisions at $\sqrt{s} = 13$ TeV*, .
- [71] CMS collaboration, *Measurements of differential Higgs boson production cross sections in the leptonic WW decay mode at $\sqrt{s} = 13$ TeV*, .
- [72] P. Bechtle, D. Dercks, S. Heinemeyer, T. Klingl, T. Stefaniak, G. Weiglein et al., *HiggsBounds-5: Testing Higgs Sectors in the LHC 13 TeV Era*, *Eur. Phys. J. C* **80** (2020) 1211, [2006.06007].
- [73] CDF collaboration, T. Aaltonen et al., *High-precision measurement of the W boson mass with the CDF II detector*, *Science* **376** (2022) 170–176.
- [74] C.-T. Lu, L. Wu, Y. Wu and B. Zhu, *Electroweak precision fit and new physics in light of the W boson mass*, *Phys. Rev. D* **106** (2022) 035034, [2204.03796].
- [75] Y.-Z. Fan, T.-P. Tang, Y.-L. S. Tsai and L. Wu, *Inert Higgs Dark Matter for CDF II W -Boson Mass and Detection Prospects*, *Phys. Rev. Lett.* **129** (2022) 091802, [2204.03693].
- [76] C.-R. Zhu, M.-Y. Cui, Z.-Q. Xia, Z.-H. Yu, X. Huang, Q. Yuan et al., *GeV antiproton/ γ -ray excesses and the W -boson mass anomaly: three faces of $\sim 60 - 70 GeV$ dark matter particle?*, 2204.03767.
- [77] B.-Y. Zhu, S. Li, J.-G. Cheng, R.-L. Li and Y.-F. Liang, *Using γ -ray observation of dwarf spheroidal galaxy to test a dark matter model that can interpret the W -boson mass anomaly*, 2204.04688.
- [78] H. Song, W. Su and M. Zhang, *Electroweak Phase Transition in 2HDM under Higgs, Z -pole, and W precision measurements*, 2204.05085.
- [79] H. Bahl, J. Braathen and G. Weiglein, *New physics effects on the W -boson mass from a doublet extension of the SM Higgs sector*, *Phys. Lett. B* **833** (2022) 137295, [2204.05269].
- [80] Y. Heo, D.-W. Jung and J. S. Lee, *Impact of the CDF W -mass anomaly on two Higgs doublet model*, *Phys. Lett. B* **833** (2022) 137274, [2204.05728].
- [81] K. S. Babu, S. Jana and V. P. K., *Correlating W -Boson Mass Shift with Muon $g-2$ in the Two Higgs Doublet Model*, *Phys. Rev. Lett.* **129** (2022) 121803, [2204.05303].
- [82] T. Biekötter, S. Heinemeyer and G. Weiglein, *Excesses in the low-mass Higgs-boson search and the W -boson mass measurement*, 2204.05975.
- [83] Y. H. Ahn, S. K. Kang and R. Ramos, *Implications of New CDF-II W Boson Mass on Two*

- Higgs Doublet Model*, [2204.06485](#).
- [84] X.-F. Han, F. Wang, L. Wang, J. M. Yang and Y. Zhang, *Joint explanation of W -mass and muon $g-2$ in the 2HDM**, *Chin. Phys. C* **46** (2022) 103105, [[2204.06505](#)].
- [85] G. Arcadi and A. Djouadi, *The 2HD+a model for a combined explanation of the possible excesses in the CDF M_W measurement and $(g-2)_\mu$ with Dark Matter*, [2204.08406](#).
- [86] K. Ghorbani and P. Ghorbani, *W-Boson Mass Anomaly from Scale Invariant 2HDM*, [2204.09001](#).
- [87] A. Broggio, E. J. Chun, M. Passera, K. M. Patel and S. K. Vempati, *Limiting two-Higgs-doublet models*, *JHEP* **11** (2014) 058, [[1409.3199](#)].
- [88] J. Oredsson, *2HDME : Two-Higgs-Doublet Model Evolver*, *Comput. Phys. Commun.* **244** (2019) 409–426, [[1811.08215](#)].
- [89] A. G. Akeroyd, *Fermiophobic Higgs bosons at the Tevatron*, *Phys. Lett. B* **368** (1996) 89–95, [[hep-ph/9511347](#)].
- [90] A. G. Akeroyd, *Fermiophobic and other nonminimal neutral Higgs bosons at the LHC*, *J. Phys. G* **24** (1998) 1983–1994, [[hep-ph/9803324](#)].
- [91] A. Barroso, L. Brucher and R. Santos, *Is there a light fermiophobic Higgs?*, *Phys. Rev. D* **60** (1999) 035005, [[hep-ph/9901293](#)].
- [92] L. Brucher and R. Santos, *Experimental signatures of fermiophobic Higgs bosons*, *Eur. Phys. J. C* **12** (2000) 87–98, [[hep-ph/9907434](#)].
- [93] A. G. Akeroyd, M. A. Diaz and F. J. Pacheco, *Double fermiophobic Higgs boson production at the CERN LHC and LC*, *Phys. Rev. D* **70** (2004) 075002, [[hep-ph/0312231](#)].
- [94] A. Arhrib, R. Benbrik, R. B. Guedes and R. Santos, *Search for a light fermiophobic Higgs boson produced via gluon fusion at Hadron Colliders*, *Phys. Rev. D* **78** (2008) 075002, [[0805.1603](#)].
- [95] E. L. Berger, Z. Sullivan and H. Zhang, *Associated Higgs plus vector boson test of a fermiophobic Higgs boson*, *Phys. Rev. D* **86** (2012) 015011, [[1203.6645](#)].
- [96] V. Ilisie and A. Pich, *Low-mass fermiophobic charged Higgs phenomenology in two-Higgs-doublet models*, *JHEP* **09** (2014) 089, [[1405.6639](#)].
- [97] A. Delgado, M. Garcia-Pepin, M. Quiros, J. Santiago and R. Vega-Morales, *Diphoton and Diboson Probes of Fermiophobic Higgs Bosons at the LHC*, *JHEP* **06** (2016) 042, [[1603.00962](#)].
- [98] T. Mondal and P. Sanyal, *Same sign trilepton as signature of charged Higgs in two Higgs doublet model*, *JHEP* **05** (2022) 040, [[2109.05682](#)].
- [99] K. Cheung, A. Jueid, J. Kim, S. Lee, C.-T. Lu and J. Song, *Comprehensive study of the light charged Higgs boson in the type-I two-Higgs-doublet model*, *Phys. Rev. D* **105** (2022) 095044, [[2201.06890](#)].
- [100] A. Djouadi, *The Anatomy of electro-weak symmetry breaking. II. The Higgs bosons in the minimal supersymmetric model*, *Phys. Rept.* **459** (2008) 1–241, [[hep-ph/0503173](#)].
- [101] C. Degrande, C. Duhr, B. Fuks, D. Grellscheid, O. Mattelaer and T. Reiter, *UFO - The Universal FeynRules Output*, *Comput. Phys. Commun.* **183** (2012) 1201–1214, [[1108.2040](#)].

- [102] A. Alloul, N. D. Christensen, C. Degrande, C. Duhr and B. Fuks, *FeynRules 2.0 - A complete toolbox for tree-level phenomenology*, *Comput. Phys. Commun.* **185** (2014) 2250–2300, [[1310.1921](#)].
- [103] J. Alwall, M. Herquet, F. Maltoni, O. Mattelaer and T. Stelzer, *MadGraph 5 : Going Beyond*, *JHEP* **06** (2011) 128, [[1106.0522](#)].
- [104] NNPDF collaboration, R. D. Ball et al., *Parton distributions from high-precision collider data*, *Eur. Phys. J. C* **77** (2017) 663, [[1706.00428](#)].
- [105] J. Baglio, A. Djouadi, R. Gröber, M. M. Mühlleitner, J. Quevillon and M. Spira, *The measurement of the Higgs self-coupling at the LHC: theoretical status*, *JHEP* **04** (2013) 151, [[1212.5581](#)].
- [106] ATLAS collaboration, *Measurement prospects of the pair production and self-coupling of the Higgs boson with the ATLAS experiment at the HL-LHC*, .
- [107] A. Ballestrero, G. Bevilacqua and E. Maina, *A Complete parton level analysis of boson-boson scattering and ElectroWeak Symmetry Breaking in $lv + \text{four jets}$ production at the LHC*, *JHEP* **05** (2009) 015, [[0812.5084](#)].
- [108] S. Jung, Z. Liu, L.-T. Wang and K.-P. Xie, *Probing Higgs boson exotic decays at the LHC with machine learning*, *Phys. Rev. D* **105** (2022) 035008, [[2109.03294](#)].
- [109] TLEP DESIGN STUDY WORKING GROUP collaboration, M. Bicer et al., *First Look at the Physics Case of TLEP*, *JHEP* **01** (2014) 164, [[1308.6176](#)].
- [110] J. Gao, *CEPC and SppC Status — From the completion of CDR towards TDR*, *Int. J. Mod. Phys. A* **36** (2021) 2142005.
- [111] CEPC STUDY GROUP collaboration, M. Dong et al., *CEPC Conceptual Design Report: Volume 2 - Physics & Detector*, [1811.10545](#).
- [112] R. B. Palmer, J. S. Berg, R. C. Fernow, J. C. Gallardo, H. G. Kirk, Y. Alexahin et al., *A Complete Scheme of Ionization Cooling for a Muon Collider*, *Conf. Proc. C* **070625** (2007) 3193, [[0711.4275](#)].
- [113] J. P. Delahaye, M. Diemoz, K. Long, B. Mansoulié, N. Pastrone, L. Rivkin et al., *Muon Colliders*, [1901.06150](#).
- [114] K. M. Black et al., *Muon Collider Forum Report*, [2209.01318](#).
- [115] T. P. Cheng, E. Eichten and L.-F. Li, *Higgs Phenomena in Asymptotically Free Gauge Theories*, *Phys. Rev. D* **9** (1974) 2259.
- [116] H. Komatsu, *Behavior of the Yukawa and the Quartic Scalar Couplings in Grand Unified Theories*, *Prog. Theor. Phys.* **67** (1982) 1177.